



## Characterization of infrasound from lightning

J. D. Assink,<sup>1</sup> L. G. Evers,<sup>1</sup> I. Holleman,<sup>2</sup> and H. Paulssen<sup>3</sup>

Received 3 April 2008; revised 12 June 2008; accepted 25 June 2008; published 2 August 2008.

[1] During thunderstorm activity in the Netherlands, electromagnetic and infrasonic signals are emitted due to the process of lightning and thunder. It is shown that correlating infrasound detections with results from an electromagnetic lightning detection network is successful up to distances of 50 km from the infrasound array. Infrasound recordings clearly show blastwave characteristics which can be related to cloud-ground discharges, with a dominant frequency between 1–5 Hz. Amplitude measurements of CG discharges can partly be explained by the beam pattern of a line source with a dominant frequency of 3.9 Hz, up to a distance of 20 km. The ability to measure lightning activity with infrasound arrays has both positive and negative implications for CTBT verification purposes. As a scientific application, lightning studies can benefit from the worldwide infrasound verification system. **Citation:** Assink, J. D., L. G. Evers, I. Holleman, and H. Paulssen (2008), Characterization of infrasound from lightning, *Geophys. Res. Lett.*, 35, L15802, doi:10.1029/2008GL034193.

### 1. Introduction

[2] Associating infrasound with lightning activity has been discussed in various theoretical and observational papers in the past. A thermally driven expanding channel model is proposed by *Few* [1969], describing the generation of a blastwave due to lightning channel heating. The model approximates measured lightning spectra, with a dominant frequency content from 10 to 150 Hz. In contrast, the electrostatic mechanism proposed by *Dessler* [1973] predicts rarefaction pulses, restoring the pressure equilibrium in a thundercloud where charge is removed. It is shown that these pulses propagate along vertical raypaths. Estimates on power spectra are given in the frequency range of 0.2–2 Hz.

[3] *Holmes et al.* [1971] analyze power spectra of thunderstorms and observe differences between cloud-cloud (CC) and cloud-ground (CG) discharges. Most of the CG spectrum is explained by the expanding channel model. The electrostatic model explains CC spectra fully and CG spectra partly. Further support for the electrostatic model is given in studies by *Bohannon et al.* [1977] and *Balanchandran* [1979].

[4] *Beasley et al.* [1976] report on a poor spatial and temporal correlation between electromagnetic (EM) and infrasonic signals, thereby concluding that the source of lightning associated infrasound is not likely electrostatical.

[5] *Holleman et al.* [2006] describe the validation of a Surveillance et Alerte Foudre par Interférométrie Radioélectrique (SAFIR) EM lightning detection network. Infrasound detections appeared to correlate well with SAFIR detections.

[6] The relationship between observed infrasound and EM signals is further explored in this study. Infrasound detections correlated to SAFIR detections are analyzed with respect to detection parameters and waveform content in order to get insight into the potential use of infrasound as a means for characterizing lightning. From a Comprehensive Nuclear-Test-Ban Treaty (CTBT) [see *Preparatory Commission for the Comprehensive Nuclear-Test-Ban Treaty Organization*, 1997] verification perspective, we note that lightning induced infrasound may increase the false alarm rate for explosions in the same frequency band. However, most signals of CTBT interest have longer dominant periods.

[7] Infrasound is also associated to turbulence in large thunderstorms [*Bowman and Bedard*, 1971] and to sprites, high-altitude discharges [*Farges et al.*, 2005; *Liszka and Hobara*, 2006]. This article will discuss CC and CG induced infrasound.

### 2. Methods

#### 2.1. Infrasound Detections

[8] Two infrasound arrays, DBN and EXL, are used for this study. The distance between these arrays is 145 km. Their respective locations and array designs are provided in Figure 1. Each array consists of six microbarometers, which measure pressure variations in the frequency band from 0.002 to 20 Hz. Each microbarometer is connected to six porous hoses in a star-like configuration to reduce wind-noise. Events are detected using the Fisher detector, a multiple-signal correlator based on statistical estimates of signal and noise in a Fisher ratio (F). The Fisher detector is defined in both time [*Melton and Bailey*, 1957] and frequency domains [*Smart and Flinn*, 1971].

[9] The highest F for an event is found for the best beam, for which all input signals are time-aligned, thereby resolving event slowness  $\vec{p}$  and hence its source parameters, back-azimuth  $\phi$  and apparent velocity  $c_{app}$ . Fisher detection is carried out in bins of 1.6 seconds; subsequent bins have 50% overlap. The infrasonic waveforms are detrended and band pass filtered between 1.0 and 10 Hz.

[10] The detection threshold is set by considering the relation between signal-to-noise power ratio (*snrp*) and F:  $snrp = \frac{1}{C}(F - 1)$ . Here, C is the number of array elements.

#### 2.2. EM Detections

[11] The SAFIR network consists of four detection stations in the Netherlands and three in Belgium see Figure 1. A station consists of five very high frequency (VHF) dipole antennas placed on a circular plane and one low frequency (LF) antenna, all sensitive to electromagnetic waves. The

<sup>1</sup>Department of Seismology, Royal Netherlands Meteorological Institute, De Bilt, Netherlands.

<sup>2</sup>Department of Weather Research, Royal Netherlands Meteorological Institute, De Bilt, Netherlands.

<sup>3</sup>Department of Seismology, Utrecht University, Utrecht, Netherlands.

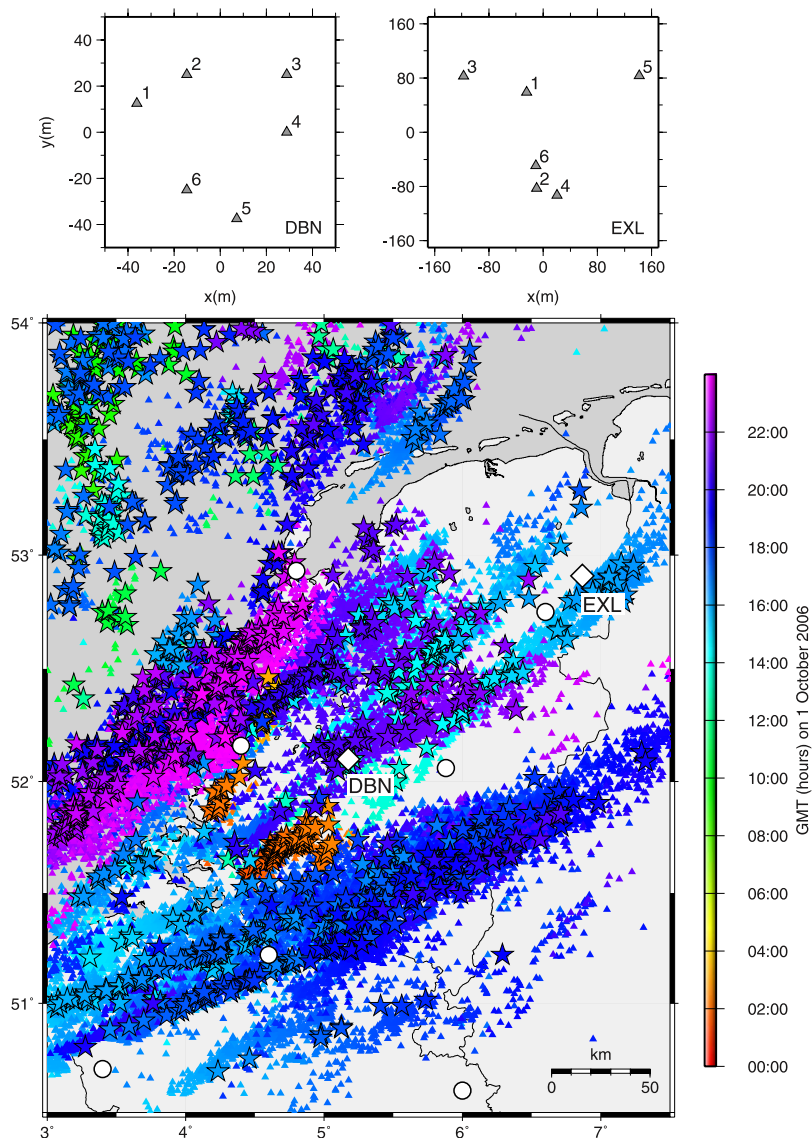


**Figure 1.** Map of the Netherlands, showing lightning activity on 1 October 2006. The stars represent CG discharges, the triangles represent CC discharges, detected by SAFIR. Color represents time of discharge, given in GMT. The SAFIR lightning detection network is plotted with circles; infrasound arrays DBN (De Bilt) and EXL (Exloo) are given, including array lay-out.

VHF array is used to detect and localize CC discharges by means of interferometry and cross bearing the observations at different stations. CG discharges are detected and localized by means of time-of-arrival and hyperbolic intersection methods. For this purpose, the LF antennas are used. To avoid ambiguity, a minimum of four stations is needed to detect the CG discharge. The SAFIR central processor gathers event information from all stations in the network and provides location, time and error of detection and for CG discharges electrical current peak, rise- and decay time values [Beekhuis and Holleman, 2004].

### 3. Observations

[12] On 1 October 2006, a severe thunderstorm passed over the Netherlands from the Southwest to the Northeast as shown in Figure 1. This day is taken to elucidate the detectability of lightning activity using infrasound arrays.

In Figures 1 and 2, CC and CG discharges are represented by triangles and stars, respectively.

[13] Figure 2 shows a joint EM-infrasound analysis for DBN, as a function of time. Figure 2a shows the distance of CC and CG discharges to DBN. The thunderstorm approaches DBN until 13h45 and then moves away. Several CG discharges occur nearby DBN.

[14] Figure 2b plots the SAFIR detections in terms of back-azimuth to DBN, with infrasound detections overlaid. Infrasound detections are represented by small circles. Color is determined by the *snrp* of the detection, according to the scale on the right. Only events with a *snrp* larger than 1 are plotted. For DBN, the uncertainty in resolved back-azimuths is estimated at  $\pm 1^\circ$ , around  $f = 3$  Hz [Evers and Haak, 2003]. Back-azimuths of SAFIR detections and highly coherent infrasound detections correlate very well between 13h20 and 14h25 GMT. During this interval, lightning discharges are detected at distances of up to

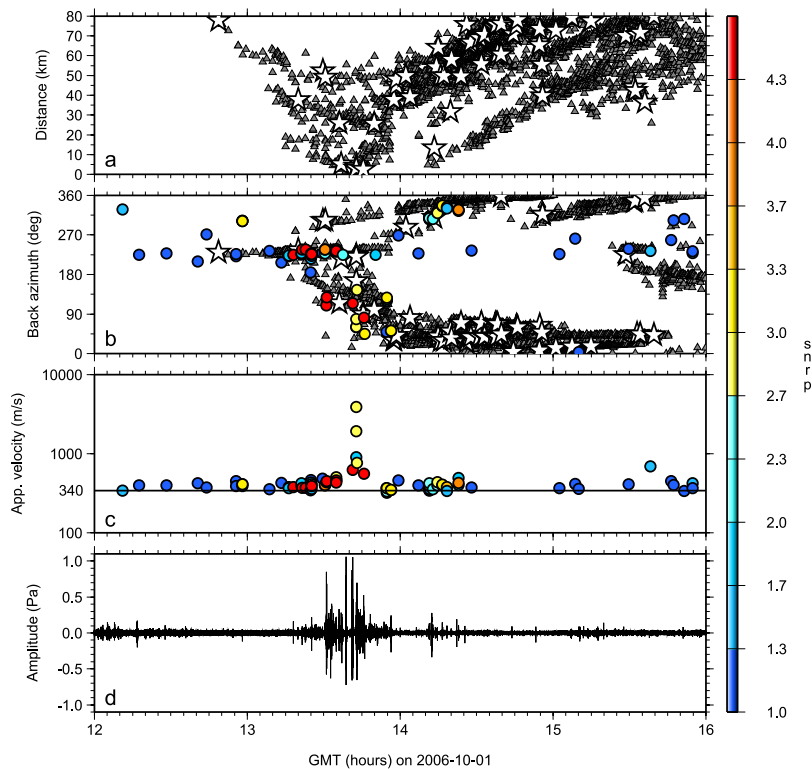


**Figure 2.** Joint EM-infrasound analysis on 1 October 2006 for DBN array. SAFIR lightning locations are given in terms of (a) distance and (b) back-azimuth to DBN. CG discharges are denoted by stars, CC discharges by triangles. Infrasound detections are plotted as circles, in terms of apparent velocity and back-azimuth to DBN. Back-azimuth values for SAFIR and infrasound are presented together in Figure 2b. (c) Apparent velocity of infrasound detections. The circles are colored, based on the coherency of the infrasound detection, which is expressed by the snrp (scale to the right). (d) Phased array sum for the best beam.

50 km from the infrasonic array. The degree of signal correlation for infrasound from discharges located at distances beyond 50 km is small, e.g. after 14h25 GMT.

[15] Figure 2c shows the apparent velocity of infrasound detections. A clear correlation exists between nearby lightning activity and coherent infrasound with high apparent velocity values. High apparent velocity corresponds to more vertical incidence. Infrasound detections associated with more distant strikes arrive with apparent velocities of about 340 m/s, typical of sound speeds in the boundary layer.

[16] The infrasonic best beam, formed with  $\vec{p}$  at maximum F, is presented in Figure 2d. Several short-lived, isolated events are visible; their amplitude levels appear to be proportional to the distance of the lightning discharge from the array.

[17] Figure 3 zooms in on the infrasound best beam, showing several blastwaves during an interval of nearby lightning activity. Blast waves can be described by an initial sharp increase in pressure, followed by a sharp drop. An ‘overshoot’, a small rise in pressure, can be present in the waveform, before the pressure level returns to equilibrium.

[18] Theory predicts blastwaves [F<sub>ew</sub>, 1969] for CG discharges and rarefaction pulses [D<sub>essler</sub>, 1973] for CC discharges. The unique presence of blastwaves in the best beam is an indicator that the recorded infrasound is due to CG discharges. We have not identified CC discharges in our infrasound measurements. The approximate ratio of CG to CC discharges is 1:20, according to the SAFIR dataset.

[19] For a spectrogram of the best beam, the S-transform is used. The S-transform, introduced by *Stockwell et al.* [1996], offers a better time-frequency representation compared to spectrogram methods as the short-time Fourier transform. The spectrogram is calculated with a frequency dependent time-window rather than with a fixed width time-window. The spectral content of the blastwaves is mostly in the lower frequency band of 1–5 Hz.

[20] It is demonstrated that a correlation exists between infrasonic and electromagnetic signals from lightning. Localization of discharges could be achieved by cross bearing the back azimuths observed at different arrays, however, attempts have been unsuccessful yet.

#### 4. Attenuation

[21] The best beam as given in Figure 2 reveals that an attenuation relation exists between infrasound amplitude and the distance of lightning activity to DBN. The attenuation relation is further examined in this section, to get insight in theoretical models of lightning. Only CG discharges are considered, because the associated infrasound signal can be recognized and a measure of strength can be provided by the SAFIR system.

[22] Infrasound amplitudes are picked for associated CG discharges in a radius of 50 km around infrasound arrays DBN and EXL. A list of CG discharges with time, location and discharge strength is provided by the SAFIR network.

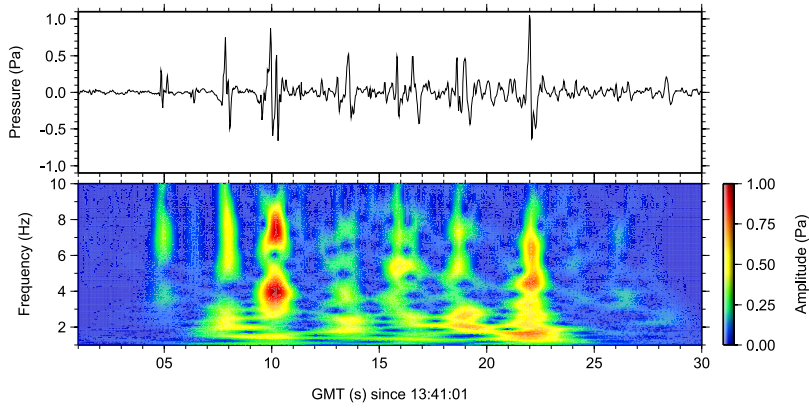


**Figure 3.** Typical infrasound best beam during nearby lightning activity. The best beam shows several blastwaves, which are associated with lightning discharges. The lower plot shows the time-frequency representation of the best beam, using the S-transform.

In order to associate infrasound with a particular SAFIR detection, infrasound recordings are searched for coherent blastwaves at  $t = t_{SAFIR} + \frac{d}{c} + \Delta t$ ;  $d$  is the distance between the CG discharge and the infrasound array,  $c$  is the speed of sound, estimated at 340 m/s and  $\Delta t$  is the allowed deviation in time,  $\pm 5$  s. Infrasound back-azimuth (observed) is allowed to deviate up to  $10^\circ$  from the back-azimuth of the SAFIR detection to the infrasound array (theoretical). A direct wave propagation path is assumed.

[23] For all array elements, peak and trough of the blastwave are picked, so that average RMS air pressure and frequency can be calculated. The sound energy density, a measure for sound energy at a given point, is calculated, using equation (1).

$$E = \frac{p^2}{\rho_0 c^2 I_{\max}^2 \Delta \tau} \quad (1)$$

[24] Here,  $E$  represents normalized sound energy density [see Kinsler *et al.*, 1999],  $p$  air pressure,  $\rho_0$  air density,  $c$  speed of sound,  $I_{\max}$  maximum CG discharge current and  $\Delta \tau$  duration time of CG discharge. The latter two quantities are measured by SAFIR and make up the measure for CG strength. Thus, sound energy is normalized for CG strength.

[25] Figure 4 shows an exponential decrease in sound energy density with increasing distance to the infrasound array. The dominant frequency is between 1 and 5 Hz, which is consistent with the spectral representations given in the previous section. A decrease in dominant frequency value is to be observed with increasing array distance. The deviation in theoretical back-azimuth and observed back-azimuth is  $4.6 \pm 3.2^\circ$ .

[26] Attenuation is the dissipation of wave energy because of geometrical spreading and the absorbing properties of the atmosphere. Bass [1980] reports on the propagation of thunder and demonstrates that atmospheric absorption and surface effects have major effects on the propagation of audible thunder. These effects are negligible for the infrasonic band. Volland [1982] models atmospheric absorption by incorporating molecular viscosity, heat conduction and molecular attenuation effects. It is shown that for severe weather conditions, atmospheric attenuation is

negligible for frequencies below 100 Hz, as it is for the regional character of this study.

[27] The results can be explained in terms of geometrical spreading of the beam patterns for a line source. The pressure field of a continuous line source with length  $L$  and radius  $a$  is given by Kinsler *et al.* [1999] by:

$$p(r, \theta, t) = \frac{i}{2} \rho_0 c \frac{Q}{\lambda r} \frac{\sin v(\theta)}{v(\theta)} e^{i(\omega t - kr)}, \theta = \arctan\left(\frac{r}{L}\right) \quad (2)$$

[28] In equation (2),  $\rho_0$  and  $c$  are ambient air density and sound speed, respectively. The source strength is expressed by  $Q = U_0 2\pi a L$  in which  $U_0$  is a source term. A beam pattern with interfering nodal surfaces is predicted from this theory; the number of nodal surfaces is controlled through the factor  $v(\theta) = \frac{1}{2} k L \sin \theta$ , where  $k = \frac{1}{\lambda}$  represents wavenumber.

[29] The normalized source energy as a function of distance is modelled by a line source with  $L = 4$  km,  $c = 340$  m/s and  $\rho_0 = 1.2$  kg/m<sup>3</sup> at frequency  $f = 3.9$  Hz and plotted in Figure 4 on top of the measurements. The mentioned parameters are well constrained and set to realistic tropospheric conditions. Frequency  $f = 3.9$  Hz is the average frequency for the measurements of Figure 4. Source parameters  $U_0$  and  $a$  are not well constrained; these parameters are combined into one free parameter to fit the model to the data. Although the expression of the continuous line source includes a time-dependency, the line source as modelled in Figure 4 is evaluated with  $t = 0$  s, since the source is of short duration.

[30] Up to 20 km array distance, the model has a reasonable fit with the data. Beyond this distance, model values are higher than the measurements. The decaying trend in the far-field, which is proportional to  $\frac{1}{r}$  (dashed line in Figure 4), is equal for both model and datapoints. This feature is common to all acoustic sources [Kinsler *et al.*, 1999].

## 5. Discussion and Conclusions

[31] Localization of lightning discharges by cross bearing has been unsuccessful. Reasons are (1) the distance between DBN and EXL is too large and (2) the atmosphere is in a

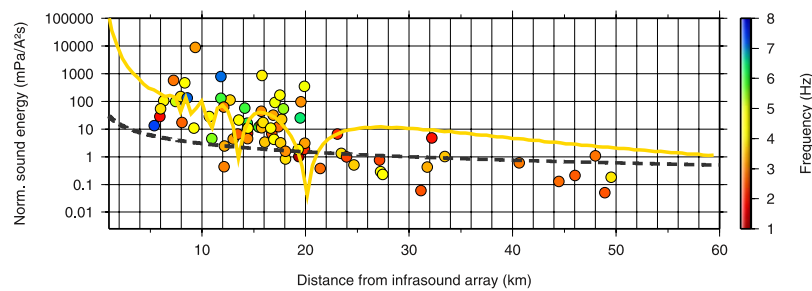


**Figure 4.** Amplitude-distance relation for infrasound from lightning, based on DBN and EXL measurements. Infrasound amplitude and array distance are related by associating infrasound to SAFIR detections. The amplitude is plotted as sound energy density, normalized for CG strength. The color of the dots is determined by the frequency of the infrasound event. The attenuation relation is modelled for a 4 km long line source in tropospheric conditions, for  $f = 3.9$  Hz; linecolor is based on the given frequency-scale. The dashed line is a  $\frac{1}{r}$  curve.

windy and turbulent state which decreases the infrasonic detection capability. The latter might also affect the ability to fully explain the observed attenuation with a line source model. Another reason for deviations could be uncertainties in CC/CG discrimination by the SAFIR system. Moreover, departures from the vertical line model could account for the current misfit, such as a segmented line source.

[32] The occurrence of multiple impulse waveforms in time around a nearby SAFIR detected CG discharge can be due to many reasons. For example, SAFIR could have missed events, it could be due to the tortuosity of a specific CG discharge, strong but distant CG discharges or CC discharges. The latter explanation is not very likely, since infrasound detections do not follow the azimuthal trend of CC discharges during nearby CC activity.

[33] It has been shown, that detections of electromagnetic and infrasonic signals from lightning show high correlations up to distances of 50 km. For 104 CG discharges around DBN with a peak current  $\geq 30$  kA, 84 infrasound associations could be established. Infrasonic signals from lightning can clearly be identified on the basis of their blastwave characteristics relating them to CG discharges with a dominant frequency content between 1–5 Hz. The radiation pattern of a line source, resulting from the thermally expanding lightning channel, can partly explain the observed attenuation relation. It is to be concluded, that lightning activity might alter the operation capability of infrasound stations in this specific frequency range, due to increased noise level and presence of coherent impulse-like signals during intervals of nearby lightning. Whether discrimination between signals from lightning and nuclear events is possible, should be further investigated. Oppositely, the infrasound verification network can be used for lightning studies, as it enables characterization of infrasound from lightning on a variety of geographical locations.

[34] **Acknowledgments.** The authors wish to acknowledge discussions with J. Mentink and T. van Zon (KNMI) on the subject of attenuation. The EXL array was constructed in cooperation with the astronomical sensor network LOFAR (<http://www.lofar.org>). Figures were generated with the help of Generic Mapping Tools, as described by *Wessel and Smith* [1991].

## References

Balachandran, N. K. (1979), Infrasonic signals from thunder, *J. Geophys. Res.*, *84*, 1735–1745.

- Bass, H. E. (1980), The propagation of thunder through the atmosphere, *J. Acoust. Soc. Am.*, *67*, 1959–1966.
- Beasley, W. H., T. M. Georges, and M. W. Evans (1976), Infrasound from convective storms: An experimental test of electrical source mechanisms, *J. Geophys. Res.*, *81*, 3133–3140.
- Beekhuis, H., and I. Holleman (2004), Upgrade and evaluation of a lightning detection system, *Tech. Rep. TR-268*, 17 pp., R. Neth. Meteorol. Inst., De Bilt, Netherlands.
- Bohannon, J. L., A. A. Few, and A. J. Dessler (1977), Detection of infrasonic pulses from thunderclouds, *Geophys. Res. Lett.*, *4*, 49–52.
- Bowman, H. S., and A. J. Bedard (1971), Observations of infrasound and subsonic disturbances related to severe weather, *Geophys. J. R. Astron. Soc.*, *26*, 215–242.
- Dessler, A. J. (1973), Infrasonic thunder, *J. Geophys. Res.*, *78*, 1889–1896.
- Evers, L. G., and H. W. Haak (2003), Tracing a meteoric trajectory with infrasound, *Geophys. Res. Lett.*, *30*(24), 2246, doi:10.1029/2003GL017947.
- Farges, T., E. Blanc, A. Le Pichon, T. Neubert, and T. H. Allin (2005), Identification of infrasound produced by sprites during the Sprite2003 campaign, *Geophys. Res. Lett.*, *32*, L01813, doi:10.1029/2004GL021212.
- Few, A. A. (1969), Power spectrum of thunder, *J. Geophys. Res.*, *74*, 6926–6934.
- Holleman, I., H. Beekhuis, S. Noteboom, L. G. Evers, H. W. Haak, H. Falcke, and L. Bühren (2006), Validation of an operational lightning detection system, paper presented at 19th International Lightning Detection Conference, Vaisala, Tucson, Ariz., 24–25 April.
- Holmes, C. R., M. Brook, P. Krehbiel, and R. McCrory (1971), On the power spectrum and mechanism of thunder, *J. Geophys. Res.*, *76*, 2106–2115.
- Kinsler, L. E., A. R. Frey, A. B. Coppens, and J. V. Sanders (1999), *Fundamentals of Acoustics*, pp. 177–179, John Wiley, New York.
- Liszka, L., and Y. Hobar (2006), Sprite-attributed infrasonic chirps—Their detection, occurrence and properties between 1994 and 2004, *J. Atmos. Sol. Terr. Phys.*, *68*, 1179–1188.
- Melton, B. S., and L. F. Bailey (1957), Multiple signal correlators, *Geophysics*, *22*, 565–588.
- Preparatory Commission for the Comprehensive Nuclear-Test-Ban Treaty Organization (1997), *Comprehensive Nuclear-Test-Ban Treaty (CTBT), Rep. V.97-28276*, 139 pp., Vienna.
- Smart, E., and E. A. Flinn (1971), Fast frequency-wavenumber analysis and Fisher signal detection in real-time infrasound array data processing, *Geophys. J. R. Astron. Soc.*, *26*, 279–284.
- Stockwell, R. G., L. Mansinha, and R. P. Lowe (1996), Localization of the complex spectrum: The S-transform, *IEEE Trans. Signal Process.*, *44*, 998–1001.
- Volland, H., (Ed.) (1982), *CRC Handbook of Atmospheric*, pp. 275–278, CRC Press, Boca Raton, Fla.
- Wessel, P., and W. H. Smith (1991), Free software helps map and display data, *Eos Trans. AGU*, *72*, 441.

J. D. Assink and L. G. Evers, Department of Seismology, Royal Netherlands Meteorological Institute, P.O. Box 201, NL-3730 AE De Bilt, Netherlands. (evers@knmi.nl)

I. Holleman, Department of Weather Research, Royal Netherlands Meteorological Institute, P.O. Box 201, NL-3730 AE De Bilt, Netherlands.  
H. Paulssen, Department of Seismology, Utrecht University, P.O. Box 80021, NL-3508 TC Utrecht, Netherlands.